Elastic moduli of a material containing composite inclusions: effective medium theory and finite element computations

By

E.J. Garboczi
Building and Fire Research Laboratory
National Institute of Standards and Technology
Gaithersburg, MD 20899 USA

and

J.G. Berryman
Lawrence Livermore National Laboratory
P.O. Box 808, L-200
Livermore, CA 94551-9900 USA

Reprinted from Mechanics of Materials, Vol. 33, No. 8, 455-470, 2001.

NOTE: This paper is a contribution of the National Institute of Standards and Technology and is not subject to copyright.

NIST
National Institute of Standards and Technology
Technology Administration, U.S. Department of Commerce

ELSEVIER

Mechanics of Materials 33 (2001) 455 470

MECHANICS OF MATERIALS

www.elsevier.com/locate/mechmat

Elastic moduli of a material containing composite inclusions: effective medium theory and finite element computations

E.J. Garboczi [a,*], J.G. Berryman [b]

[a] *Building Materials Division, National Institute of Standards and Technology, 100 Bureau Drive, Stop 8621, Gaithersburg, MD 20899-8621, USA*

[b] *Lawrence Livermore National Laboratory, P.O. Box 808, L-200 Livermore, CA, 94551-9900, USA*

Received 15 May 2001

Abstract

Concrete is a good example of a composite material in which the inclusions (rocks and sand) are surrounded by a thin shell of altered matrix material and embedded in the normal matrix material. Concrete, therefore, may be viewed as consisting of a matrix material containing composite inclusions. Assigning each of these phases different linear elastic moduli results in a complicated effective elastic moduli problem. A new kind of differential effective medium theory (D-EMT) is presented in this paper that is intended to address this problem. The key new idea is that each inclusion particle, surrounded by a shell of another phase, is mapped onto an effective particle of uniform elastic moduli. The resulting simpler composite, with a normal matrix, is then treated in usual D-EMT. Before use, however, the accuracy of this method must be determined, as effective medium theory of any kind is an uncertain approximation. One good way to assess the accuracy of effective medium theory is to compare to exact results for known microstructures and phase moduli. Exact results, however, only exist for certain microstructures (e.g., dilute limit of inclusions) or special choices of the moduli (e.g., equal shear moduli). Recently, a special finite element method has been developed that can compute the linear elastic moduli of an arbitrary digital image in 2D or 3D. If a random microstructure can be represented with enough resolution by a digital image, then its elastic moduli can be readily computed. This method is used, after proper error analysis, to provide stringent tests of the new D-EMT equations, which are found to compare favorably to numerically exact finite element simulations, in both 2D and 3D, with varying composite inclusion particle size distributions. © 2001 Published by Elsevier Science Ltd.

Keywords: Fnite element; Effective medium theory; Concrete; Microstructure; Random elastic

1. Introduction

Concrete is a composite material. A typical mixture contains a cement paste (=hydrated cement) matrix and inclusion particles of various sizes, ranging from the smallest sand grains of diameter 100 μm, to the largest rocks of diameter 10–20 mm. But concrete is not just a simple two-phase composite. Upon closer examination, one finds that the presence of the grains in the paste changes a thin layer of matrix material surrounding each inclusion. The cement paste matrix in this shell is different, usually more porous, than the bulk of the surrounding cement paste matrix. Typical widths of this layer are in the range 10–30 μm. This

* Corresponding author. Tel.: +301-975-6707; fax: +301-990-6891.

E-mail address: edward.garboczi@nist.gov (E.J. Garboczi).

0167-6636/01/$ - see front matter © 2001 Published by Elsevier Science Ltd.
PII: S0167-6636(01)00067-9

layer is often called the interfacial transition zone (ITZ) (Bentz et al., 1993; Scrivener, 1989; Scrivener and Nemati, 1996; Garboczi and Bentz, 1991).

Concrete, therefore, consists of at least three distinct types of constituents. If the altered shell of matrix material is associated with the grains, the point of view may be taken (and this will become our point of view) that concrete consists of a matrix material containing *composite* inclusions. Assigning each of these phases different isotropic linear elastic moduli results in a complicated effective elastic moduli problem.

In fact, the problem is still more complicated. The "shell" around each inclusion actually contains a gradient of properties, since the cement paste matrix density is least at the particle surface and increases outwards to the full matrix density (Scrivener, 1989; Shane et al., 2000; Bentz et al., 1992). If the inclusions in concrete are modeled as spheres, which is a good approximation for many concrete mixtures, then the dilute limit, with a single spherical inclusion surrounded by a thin layer containing a spherically symmetric gradient of point-wise isotropic elastic properties, can be handled exactly (Garboczi and Bentz, 1997; Herve and Zaoui, 1993; Iske et al., 1994; Lutz and Monteiro, 1995). But the non-dilute microstructure of concrete, with a wide particle size distribution of inclusions, each surrounded by overlapping gradients of properties, is very difficult to treat analytically, by numerical methods, or by effective medium theory (EMT). However, it has been shown that a multi-scale model can be used in order to map this complex microstructure into a simpler, but still complicated, microstructure, where the shell layers can be treated theoretically as having uniform properties (Garboczi and Bentz, 1997, 1998; Bentz et al., 1998). The three phase composite described above then becomes appropriate for the concrete elastic moduli problem, and is the focus of this paper. We note that other treatments of how to actually map interphase microstructure into effective layer properties sometimes allow for anisotropic elasticity in the interphase region (Ostoja-Starzewski et al., 1996). We restrict ourselves to isotropic elasticity in this paper.

Differential effective medium theory (D-EMT) for this three-phase microstructure has been developed previously in several ways (Cleary et al., 1980; Sheng and Callegari, 1984; Norris, 1985; Sheng, 1990, 1991; Dvorkin et al., 1999). Predictions for the electrical properties of this microstructure have recently been checked against random walk simulations (Schwartz et al., 1995; Garboczi and Berryman, 2000). These simulations are accurate and simple, but time-consuming, hence the use of effective medium theory. The most accurate D-EMT for this application was developed using a new idea in differential effective medium theory (D-EMT) (Garboczi and Berryman, 2000). The key idea was that a spherical inclusion, along with its surrounding thin shell of altered matrix material, was exactly mapped into a new, slightly larger homogenized inclusion, which included the hard but poorly conducting particle and the softer but better conducting shell, and which had a uniform conductivity. The new system of effective particles embedded in the matrix could then be treated easily using a differential effective medium theory (D-EMT).

A rather different approach to three-phase effective medium theory could be based on the self-consistent formulas of Christensen and Lo (Christensen and Lo, 1979; Christensen, 1979), but as we shall show, the method presented here has considerably more flexibility in the range of complex microstructures that can be incorporated into the model.

This new kind of D-EMT is extended to linear elastic properties in this paper. Similar to the idea used for conductivity, a spherical inclusion, with a surrounding shell layer, is mapped onto an effective particle of uniform elastic moduli. The problem then becomes a simple composite composed of spherical particles, of varying sizes and elastic moduli, embedded in a uniform matrix. This composite can then be treated in the usual D-EMT.

Except for some special models (Milton, 1985), the accuracy of most EMTs is often in doubt. From the point of view of tailoring the approximation to the specific material microstructure that we want to model, EMTs of any kind tend to be uncontrolled approximations. Checking the accuracy of an EMT by comparing its predictions to experimental results is inadequate from the

theoretical point of view because the microstructure and phase elastic moduli are usually only approximately known experimentally. Observed discrepancies could be from the EMT, or equally well could arise from the approximate knowledge of the experimental material. A more satisfactory way of assessing the accuracy of EMT is to compare to exact analytical results, where microstructure and phase moduli are controlled by the user. But exact elastic results for non-trivial microstructures are rather rare, and only exist for certain microstructures (e.g., dilute limit of inclusions) or special choices of the moduli (e.g., equal shear moduli) (Hill, 1963; Garboczi, 1998). In the case of conductivity, the D-EMT results could be checked on model concrete microstructures using accurate random walk simulations (Garboczi and Berryman, 2000). Recently, a special finite element method has been described that can compute the linear elastic moduli of an arbitrary digital image in 2D or 3D (Garboczi and Day, 1995). This method is used, after proper error analysis, to provide stringent tests of the new D-EMT equations. The results are found to compare favorably with the essentially exact finite element calculations, in both 2D and 3D, with a variety of simple inclusion size distributions.

2. Differential effective medium theory and effective particle mapping

D-EMT (McLaughlin, 1977; Berryman, 1995) was chosen as the best candidate for the composite inclusion problem for the following reason. The accuracy of an EMT is often linked to how well its percolation properties match those of the experimental system being considered (Schwartz et al., 1995; Xia and Thorpe, 1988; Berge et al., 1993). In D-EMT, the inclusions are always discontinuous, and the matrix is always continuous. Concrete has the same properties since the granular aggregate is fully surrounded by the cementing matrix material. Thus, the microstructures of the theory and the problem of interest are well matched. Furthermore, we want to be able to incorporate a range of sizes of particles into the theory in a controlled way. It is not clear how to do this in a self-consistent three-component model (Christensen and Lo, 1979), but we will show that this is not difficult to achieve with the present approach.

The standard D-EMT is a two-phase theory, or rather two topological phases, since each inclusion can be a different phase through having different elastic properties. In the present case, the thin shell of disturbed material around each granular inclusion causes conceptual problems for D-EMT, since it introduces at least one more topological phase. To make use of D-EMT in this setting, the following question arises: Should this shell should be treated as part of the inclusion, or as part of the matrix?

Since the shell regions, disregarding possible overlaps between shells, will necessarily assume the same shape as the spherical inclusion particles, the option of making the shell regions part of the inclusions seems the most appropriate one. This is accomplished by mapping each spherical inclusion particle, together with its accompanying shell, into a single effective particle, with size sufficient to incorporate both and with uniform elastic properties. This idea is illustrated in Fig. 1, and will be developed more fully below. Thus, the effective medium theory that we develop will be for a material having a matrix that contains spherical composite inclusions.

In what follows in Section 2, first the standard two-phase D-EMT is described. Then the effective particle mapping is discussed, showing how the three phase model of concrete can be reduced to a

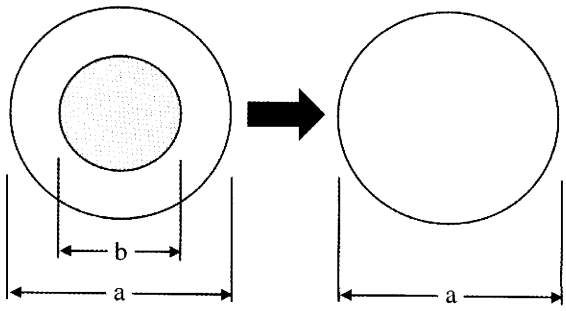

Fig. 1. The mapping of a composite inclusion particle into an effective particle whose diameter is that of the outer shell. The figure shows a cross-section of a sphere (or a circle) taken through the center.

two topological phase model, which is more readily handled with D-EMT. Then we show how the standard D-EMT can be modified so as to use the effective particles, producing a new D-EMT result.

2.1. Standard D-EMT

In the usual D-EMT (McLaughlin, 1977), when a particle with elastic moduli K_p and G_p is embedded in a matrix with elastic moduli K_m and G_m, the dilute limit is used to generate an approximate equation that can be solved for the effective elastic moduli (McLaughlin, 1977). In the dilute limit, the value of c, the volume fraction of particles, is small enough so that the particles do not influence each other. The effective elastic moduli, K and G, are then given by Torquato (1991)

$$K = K_m + K_m k(K_p, K_m, G_m)c + \mathrm{O}(c^2), \tag{1}$$

$$G = G_m + G_m g(G_p, K_m, G_m)c + \mathrm{O}(c^2), \tag{2}$$

where k and g are dimensionless coefficients. These coefficients are often called the dilute limit slopes or the intrinsic moduli (Douglas and Garboczi, 1995), and are functions of both the shape of the particle and the moduli shown. The higher-order terms in the c expansion come from interactions between particles, and so are negligible in the dilute limit.

For circular particles in a 2D matrix and spherical particles in a 3D matrix, these dilute limits are known. For circular particles in 2D, the values of k and g are:

$$k = \frac{(K_m + G_m)(K_p - K_m)}{K_m(K_p + G_m)}, \tag{3}$$

$$g = \frac{2(K_m + G_m)(G_p - G_m)}{G_m(K_m + G_p) + G_p(K_m + G_m)}. \tag{4}$$

For spherical particles in 3D, the values of k and g are:

$$k = \frac{(K_m + \frac{4}{3}G_m)(K_p - K_m)}{K_m(K_p + \frac{4}{3}G_m)}, \tag{5}$$

$$g = \frac{5(K_m + \frac{4}{3}G_m)(G_p - G_m)}{3G_m(K_m + \frac{8}{9}G_m) + 2G_p(K_m + 2G_m)}. \tag{6}$$

The dilute limits are now used to generate approximate differential equations suitable to estimate the elastic moduli when arbitrary amounts of the included phase are introduced into the matrix. Suppose that a non-dilute volume fraction c of particles have been placed in the matrix. The effective elastic moduli of the entire composite system are now $K = K(\phi)$ and $G = G(\phi)$, where $\phi = 1 - c$ is the matrix volume fraction. The resulting system of matrix plus particles is treated as a homogeneous material. Suppose then that more particles are added by removing a differential volume element, $\mathrm{d}V$, from the homogeneous material, and replacing it by an equivalent volume of the inclusion phase. The new elastic moduli, $K + \mathrm{d}K$ and $G + \mathrm{d}G$, are given in the dilute limit by

$$K + \mathrm{d}K = K + K\,k(K_p, K, G)\frac{\mathrm{d}V}{V}, \tag{7}$$

$$G + \mathrm{d}G = G + G\,g(G_p, K, G)\frac{\mathrm{d}V}{V}, \tag{8}$$

where V is the total volume and $k(K_p, K, G)$ and $g(G_p, K, G)$ are the same quantities as those in Eqs. (1) and (2), but with the replacement $K_m \to K$ and $G_m \to G$. This is the key approximation that is made in order to generate the standard two-component D-EMT. The variable $\mathrm{d}V/V$ is now playing the role of the dilute volume fraction c in Eqs. (1) and (2). When the volume element $\mathrm{d}V$ is removed, only a fraction ϕ is actually matrix material, so that the actual change in the matrix volume fraction, $\mathrm{d}\phi$, is given by

$$\mathrm{d}\phi = -\phi\frac{\mathrm{d}V}{V}. \tag{9}$$

Making this substitution, Eqs. (7) and (8) reduce to the coupled set of equations

$$\begin{aligned} \frac{\mathrm{d}K}{\mathrm{d}\phi} &= -kK/\phi, \\ \frac{\mathrm{d}G}{\mathrm{d}\phi} &= -gG/\phi. \end{aligned} \tag{10}$$

These equations are coupled via the k and g terms, which depend on the values of K and G for the matrix at the given value of ϕ.

The above has been written for a single size inclusion. For a size distribution of inclusion particle diameters $\{b_j\}$, the theory is only slightly more complicated. Some composites might also have different elastic moduli for different sizes of particles. A general way of characterizing the inclusion size distribution is by specifying the diameter of each type, d_j, $j = 1, M$, where M is the number of different kinds of particles, and f_j is the fraction of the total inclusion volume that is taken up by the jth kind of particle, with $\sum_j f_j = 1$. The elastic moduli of the jth kind of particle is given by K_j and G_j.

It makes some difference, mathematically, to the final results just how (i.e., in what order) the various inclusion types are mixed into the composite (Norris, 1985). One might put all the smallest particles in first, then all of the next size particle, and so on, with the largest particles the last to be put in, or vice versa. We have chosen to assume the inclusion distribution is maintained as a fixed quantity throughout the mixing process, and have ignored other procedures. This means that the complete size distribution of inclusions is used each time particles are mathematically added. In the case of concrete, one can picture putting all the sand and rocks into a large container, throughly mixing the inclusions, then scooping out the mixture into the cement paste matrix. The way this affects the D-EMT is seen in the dilute limit, or the values of k and g, which become $\langle k \rangle = \sum_j f_j k_j$ and $\langle g \rangle = \sum_j f_j g_j$. These slopes are first averaged over the inclusion particle size distribution before being used in the formula for the dilute limit. The D-EMT is then built up the same way as for a single kind of particle, but using the average slopes.

2.2. Effective particle mapping

It has been long known that a spherical particle, surrounded by a spherical shell of different elastic moduli, can be exactly mapped into a new, uniform property spherical particle, which is as large as the old particle plus shell combined (Hashin, 1962; Christensen, 1979, 1990). This can also be done for a circular particle surrounded by a circular shell. Of course, in concrete some of the shells overlap. In this effective particle mapping, overlaps are ignored, so that each particle is assumed to have a complete, isolated shell around it. This procedure can actually be done for n such spherical shell layers (Herve and Zaoui, 1993; Iske et al., 1994), though this paper restricts its analysis to a single layer around a spherical particle.

Let the interior particle be phase 3, with diameter b, and the shell material be phase 2, with outer diameter a. The phase label 1 is reserved for the matrix. Fig. 1 shows a schematic of such a mapping. The reference (Christensen, 1990) contains the formulas for such a mapping in 3D, for both the effective properties K and G, and for G in 2D. The 2D mapping for K is also included below. Note that in Christensen (1990), in 3D, label i is the same as 3 here, and label m is the same as 2 here. In 2D, label f is the same as 3 here, and label m is the same as 2 here. Also, in both 2D and 3D, ν_i is the Poisson's ratio for phase i.

The 3D results are presented first. The effective G is the solution to the following quadratic equation (the positive square root is the physical choice):

$$A(G/G_2)^2 + 2B(G/G_2) + C = 0 \tag{11}$$

with the coefficients given by

$$\begin{aligned}
A &= 8z(4-5\nu_2)\eta_\alpha p^{10/3} - 2[63z\eta_\beta + 2\eta_\alpha\eta_\gamma]p^{7/3} \\
&\quad + 252z\eta_\beta p^{5/3} - 50z(7-12\nu_2+8\nu_2^2)\eta_\beta p \\
&\quad + 4(7-10\nu_2)\eta_\beta\eta_\gamma, \\
B &= -2z(1-5\nu_2)\eta_\alpha p^{10/3} + 2[63z\eta_\beta + 2\eta_\alpha\eta_\gamma]p^{7/3} \\
&\quad - 252z\eta_\beta p^{5/3} + 75z(3-\nu_2)\eta_\beta\nu_2 p \\
&\quad + \frac{3}{2}(15\nu_2 - 7)\eta_\beta\eta_\gamma, \\
C &= 4z(5\nu_2-7)\eta_\alpha p^{10/3} - 2[63z\eta_\beta + 2\eta_\alpha\eta_\gamma]p^{7/3} \\
&\quad + 252z\eta_\beta p^{5/3} + 25z(\nu_2^2-7)\eta_\beta p - (7+5\nu_2)\eta_\beta\eta_\gamma, \\
\eta_\alpha &= z(7-10\nu_2)(7+5\nu_3) + 105(\nu_3-\nu_2), \\
\eta_\beta &= z(7+5\nu_3) + 35(1-\nu_3), \\
\eta_\gamma &= z(8-10\nu_2) + 15(1-\nu_2), \\
z &= G_3/G_2 - 1, \\
p &= (b/a)^3.
\end{aligned} \tag{12}$$

The effective K is given by

$$K = K_2 + \frac{p(K_3 - K_2)}{1 + (1-p)\frac{(K_3 - K_2)}{(K_2 + \frac{4}{3}G_2)}}. \tag{13}$$

For 2D, the plane strain shear modulus, μ_{23}, is used from Christensen (1990), but with the notation of this paper. The effective G is given by the solution of the following quadratic equation (in this case the negative square root is the physical choice):

$$A(G/G_2)^2 + 2B(G/G_2) + C = 0 \tag{14}$$

with the coefficients given by

$$\begin{aligned}
A &= 3p(1-p)^2(r-1)(r+\eta_3) \\
&\quad + [r\eta_2 + \eta_2\eta_3 - (r\eta_2 - \eta_3)p^3] \\
&\quad \times [p\eta_2(r-1) - (r\eta_2 + 1)], \\
B &= -3p(1-p)^2(r-1)(r+\eta_3) \\
&\quad + \frac{1}{2}[r\eta_2 + (r-1)p + 1] \\
&\quad \times [(\eta_2 - 1)(r+\eta_3) - 2(r\eta_2 - \eta_3)p^3] \\
&\quad + \frac{p}{2}(\eta_2 + 1)(r-1)[r + \eta_3 + (r\eta_2 - \eta_3)p^3], \\
C &= 3p(1-p)^2(r-1)(r+\eta_3) \\
&\quad + [r\eta_2 + (r-1)p + 1] \\
&\quad \times [r + \eta_3 + (r\eta_2 - \eta_3)p^3], \\
\eta_i &= 3 - 4\nu_i \quad \text{for } i = 2,3, \\
r &= G_3/G_2, \\
p &= (b/a)^2.
\end{aligned} \tag{15}$$

The effective K, derived independently from Christensen (1990), is given by

$$K = \frac{p(K_2 + G_2)K_3 + (1-p)(K_3 + G_2)k_2}{p(K_2 + G_2) + (1-p)(K_3 + G_2)}. \tag{16}$$

2.3. New D-EMT

The resulting effective particle is now treated as the inclusion phase in the usual D-EMT, as described above. When an inclusion particle size distribution is used, the functions k and g are averages over this size distribution, as was stated above. The differential equations can be easily solved numerically by a fourth-order Runge–Kutta method (Hildebrand, 1956; Press et al., 1988).

There are a few differences, however, involving the effective inclusion volume fraction. Each particle is now of diameter $a_j = b_j + h_j$, where h_j is the shell thickness for the jth kind of inclusion, so that the volume fraction of "effective inclusions" now goes to the renormalized value c', not c. The value of c' must be known in order to know where to terminate integration of the D-EMT differential equations, which start at $c' = 0$. Possible overlaps are ignored in this calculation. The total volume of these effective particles is equal to the original volume of inclusions, plus the volume of a complete shell around each particle. The effect of overlaps, which is fairly minor, will be discussed in a later section.

The new volume fraction of effective particles can be determined simply by considering the number of particles of a certain type. If V_j is the total volume of the jth kind of particle, and N_j is the total number of this kind of particle, then

$$N_j \frac{\pi}{6}(b_j)^3 = V_j, \tag{17}$$

and, therefore,

$$\begin{aligned}
\frac{N_j}{V}\frac{\pi}{6}(b_j)^3 &= \frac{V_j}{V} = f_j c, \\
n_j \frac{\pi}{6}(b_j)^3 &= f_j c,
\end{aligned} \tag{18}$$

where V is the total volume of the system and n_j is the number of particles of type j per unit total material volume.

The values of f_j' and c' are defined directly by writing

$$c' = \sum_{j=1}^{M} n_j \frac{\pi}{6} a_j^3, \tag{19}$$

$$f_j' = \frac{n_j a_j^3}{\sum_{i-1}^{M} n_i a_i^3}. \tag{20}$$

Combining the above equations, we can then derive forms for f_j' and c' that involve only f_j, c, and $\alpha_j = a_j^3/b_j^3$:

$$c' = c\sum_{j=1}^{M} f_j \alpha_j, \tag{21}$$

$$f_j' = \frac{f_j \alpha_j}{\sum_{i=1}^{M} f_i \alpha_i}. \tag{22}$$

It should again be noted that while the value of c was for non-overlapping inclusion particles, the value of c' is for the volume occupied by each inclusion particle and its surrounding shell, where the shell layers are assumed to not overlap. In a real concrete, these shells do overlap, which can cause percolation phenomena (Winslow et al., 1994). This treatment of the shell volume fraction is another approximation of the D-EMT method. In the numerical results described in Section 3 chosen to check the D-EMT, the shell regions actually do not overlap, and, therefore, are consistent with the assumptions built into the theory. An overlapping shell example is also chosen to show the minor difference this factor makes.

In summary, a D-EMT calculation is performed as follows. First, all the different kinds of composite inclusions are mapped to effective particles, with new moduli and sizes. Next, the inclusion particle size distribution is used to compute c' and f_j'. Finally, the differential equations in Eq. (10) are solved numerically using a fourth-order Runge–Kutta method, where the slopes $\langle k \rangle$ or $\langle g \rangle$ are averaged over the effective particle size distribution f_j'. Note that for spherical particles, the new diameters of the effective particles, a_j, do not come in explicitly into any of the equations for k and g, but only in the definitions of f_j' and c'. For many materials, including concrete, the inclusion particle size distribution is given by a sieve analysis, where partial volume fractions f_j refer to the amount lying inside a certain diameter range. This case can be easily converted to the one considered here, by dividing each range into several points, and dividing up the volume in that range appropriately. The actual FORTRAN software used to calculate the D-EMT results in this paper is freely available (Garboczi, 2001).

3. Finite element computations

A recent finite element method for digital images (Garboczi and Day, 1995) was used to generate data with which to check the results of the D-EMT. Of course, if one is going to check the D-EMT results with the finite element method results, one must ask: how accurate are the finite element method results themselves? Since these results are for concentrated, random systems, there are no exact analytical data against which to check the numerical results. Fortunately, by careful consideration of the possible sources of errors, one can establish the accuracy of the numerical data.

These numerical computations are carried out by first generating the random microstructure desired by building a periodic digital image using square pixels on a 2D square lattice or cubic pixels on a 3D cubic lattice. Each pixel is then considered to be a bi-linear element (2D) or tri-linear element (3D) (Garboczi, 1998), so that the entire digital lattice is treated as the finite element mesh. The elastic displacements are linearly extrapolated across the pixels, which is why the the pixels are called bi-linear (2D) and tri-linear (3D). The elastic equations are written as a variational principle in the elastic energy, which is then minimized over the digital lattice. The effective moduli are usually defined by a stress average, although they could be defined by an energy average (Garboczi, 1998).

Because of the structure of the algorithm, there are three main sources of error: (1) finite size effect, (2) digital resolution, and (3) statistical variation (Roberts and Garboczi, 2000). Note that another method of handling similar systems without periodic boundary conditions (Ostoja-Starzewski and Schulte, 1996) has different finite size effects. However, both methods have similar digital resolution and statistical variation errors. We have found that in digital models the resolution errors often dominate the other sources of error.

The finite size effect comes about because any given digital image, even with periodic boundary conditions, can only represent a small part of a large random solid. Here we are thinking of inclusions embedded in a matrix. There can be errors induced if the sample is not large enough to possess enough inclusions to be statistically representative. This sampling error can be assessed by running several different size samples, and seeing whether the results change between system sizes. When assessing this source of error, the inclusion size, in terms of pixels, stays the same, so that samples having larger lattices contain more inclusions.

The digital resolution error comes from using square or cubic pixels to represent the inclusions.

Even if the inclusions had the same shape as the digital lattice, there would still be a resolution error since one is representing continuum equations with a digital lattice. The size of this error can be checked by holding the number of inclusions constant, and varying the size of the lattice so that there are more or fewer pixels per unit length.

The statistical variation error source simply comes about because the systems under consideration are random ones. For a given concentration of inclusions, there are many ways in which the inclusions might be randomly arranged. Each arrangement will have somewhat different elastic moduli, in general. The size of this error source can be assessed by computing the elastic moduli of several different realizations of the same system (same size lattice, same pixel size and number of inclusions).

In what follows, all the systems shown in the figures were prepared by random sequential adsorption (Cooper, 1988), with the largest particles placed first, and then in descending order in diameter. The inner and outer particles were not allowed to overlap with any other inner or outer particle. In the placement process, a trial center was picked at random. If a particle centered at this point did not overlap any other particle, then it was placed and a new site chosen at random. If the particle did overlap another particle, then the site was abandoned and a new site was chosen at random.

Fig. 2 shows the 2D 1000^2 systems that were used to check the D-EMT results. There were three sizes of inclusions. On a 1000^2 size digital lattice, these had outer–inner diameters, in pixels, of 121–99, 91–69, and 61–39. Experience with many previous results has shown that having the diameter of the largest inclusion less than $\frac{1}{8}$ of the size of the unit cell makes any finite size effects negligible. Holding the number of inclusions fixed to assess the digital resolution error, calculations were also made at sizes of 500^2 and 2000^2. There was only 1–2% variation among the different sizes, so that the size used for all the runs was 1000^2. The statistical variation for 1000^2 size systems was very small, and so was neglected.

The inner particle had Young's modulus $E_3 = 5.0$ and Poisson's ratio $\nu_3 = 0.2$, the matrix had $E_1 = 1.0$ and $\nu_1 = 0.3$, while the shell had a Young's modulus E_2 that ranged from 0.1 to about 10.0 and a Poisson's ratio of $\nu_2 = 0.3$. Two systems were chosen, with matrix area fractions of ap-

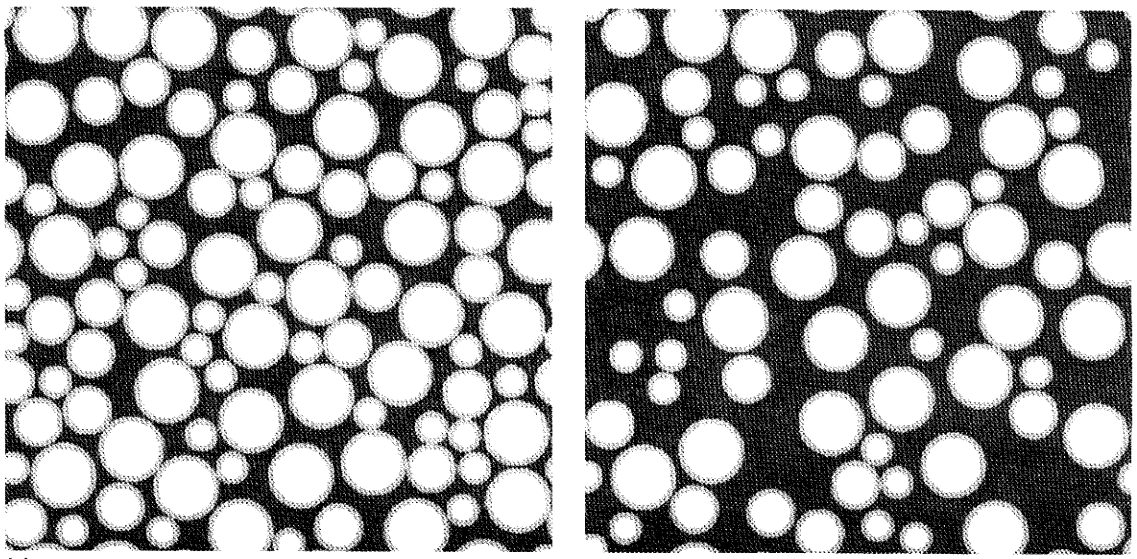

Fig. 2. Gray-scale pictures of the 2D models used to test the D-EMT predictions (non-overlapping shells). Using concrete terminology, the dark gray is the cement paste matrix, the middle gray is the ITZ regions, and the lightest gray phase is the inclusion or aggregate phase. There are three sizes of aggregates in this picture, and the matrix area fraction is 0.3 (a) and 0.5 (b).

Table 1
Parameters defining the 2D microstructures[a]

N_L	N_M	N_S	c_1	c_2	c_3
36	28	35	0.303	0.275	0.422
26	20	25	0.499	0.198	0.303

[a] N: number, L: large circles, M: medium circles, S: small circles, and c is area fraction. Phase 3 is the inner circle, phase 1 is the matrix, and phase 2 is the shell material.

proximately 0.3 and 0.5. Exact details of the microstructures considered are displayed in Tables 1 and 3. These details are given for future reference, as these highly accurate results for random, non-dilute systems are practically unique.

In 3D, there were two systems considered. The first used only one size of composite sphere, with a ratio of outer to inner diameters of 1.75. The ratio of the unit cell size to the particle outer diameter size was chosen to be about 7, which makes finite size errors negligible. The digital resolution effect was analyzed by running the exact same geometry at sizes of 100^3, 200^3, and 300^3. Fig. 3 shows four non-consecutive parallel slices of the 300^3 system. A full size range was only run for $E_2 = 0.1$ and 10.0, which were the limits of the shell stiffness. The phase moduli were the same numerically as in 2D. We found that at $E_2 = 0.1$ the resolution error was essentially 0, as all three systems gave almost exactly the same answer, within less than 0.1%. However, at $E_2 = 10.0$, there was a 3.7% drop in bulk modulus and 5.6% drop in shear modulus between the 100^3 and the 200^3 systems. There was only a 0.5% further drop in bulk modulus and 0.8% in shear modulus when going to the 300^3

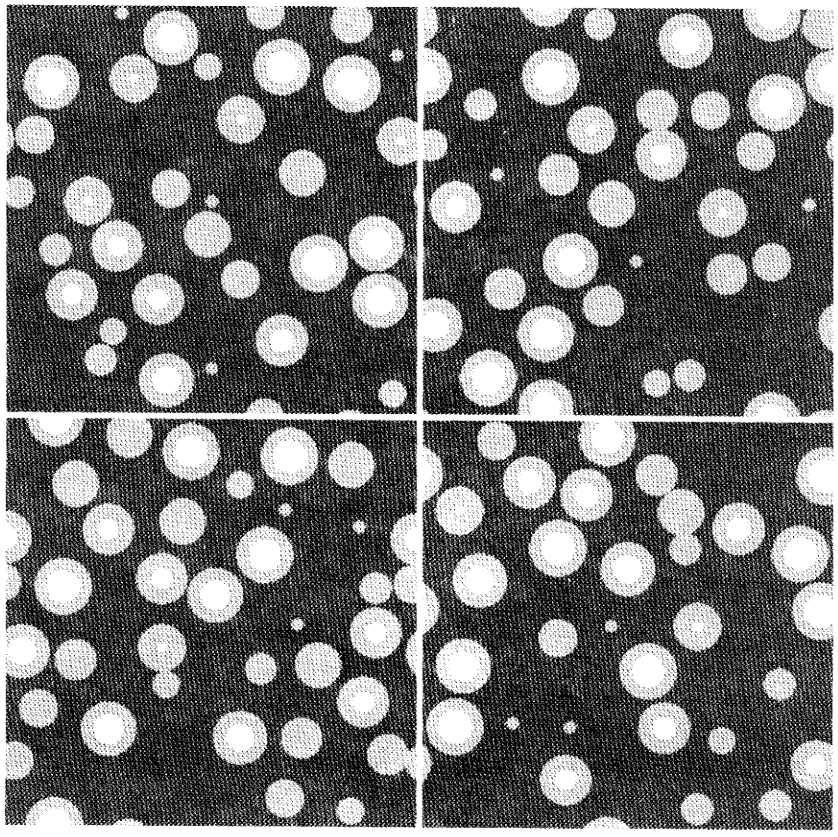

Fig. 3. Four 300^3 slices from the 3D monosize composite sphere model used to test the D-EMT predictions. Using concrete temrminology, the dark gray is the cement paste matrix, the middle gray is the ITZ regions, and the lightest gray phase is the inclusion or aggregate phase. The matrix volume fraction is 0.668.

Table 2
Parameters defining the 3D microstructures, which had either one or two sizes of spheres[a]

N_L	N_S	c_1	c_2	c_3
230		0.668	0.269	0.063
220	900	0.517	0.392	0.091

[a] The numbers are all for 200^3 systems. N: number, L: large spheres, S: small spheres, and c is volume fraction. Phase 3 is the inner sphere, phase 1 is the matrix, and phase 2 is the shell material.

system, so it was decided that the 200^3 system would give adequate accuracy for all the shell moduli. For this size system, the outer particle diameter was 28 pixels wide, while the inner diameter was 16 pixels wide. Statistical errors between configurations were negligible.

Table 3
Areas of circles and volumes of spheres used in pixels and voxels

Circle diameter	Sphere diameter	Area (pixel #)	Volume (voxel #)
121		11 476	
99		7668	
91		6488	
69		3720	
61		2912	
39		1184	
	28		11 536
	16		2176
	14		1472
	8		280

The second 3D system was 200^3 in size, and had two size spheres, with outer and inner particle diameters of 28–16 and 14–8. Judging from the data

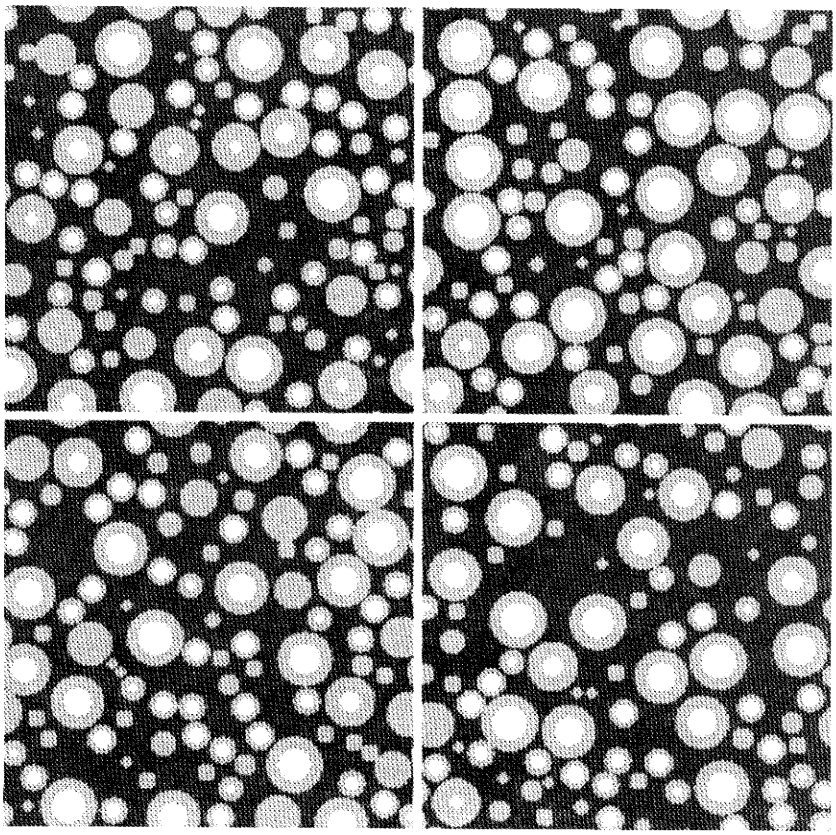

Fig. 4. Four 200^3 slices from the 3D two-size sphere model used to test the D-EMT predictions. Using concrete terminology, the dark gray is the cement paste matrix, the middle gray is the ITZ regions, and the lightest gray phase is the inclusion or aggregate phase. The matrix volume fraction is 0.517.

obtained on the single-sphere results, this choice should also have given adequate accuracy, though it was not as carefully checked as were all the other systems. The detailed parameters used for both 3D systems are presented in Tables 2 and 3. Fig. 4 shows four parallel non-consecutive slices of the 200^3 system used.

4. D-EMT results

The D-EMT equations were solved for the four (two 2D, two 3D) different microstructures for which finite element results were obtained. By varying both the microstructure and the shell stiffness, a range of data was obtained to provide a rigorous test of the D-EMT results.

Figs. 5 and 6 show the comparison between the finite element results for the 2D microstructures (symbols) and the numerically integrated D-EMT results (lines). Both graphs show excellent agreement, with the best agreement being at the greater matrix area fraction (Fig. 6). This is not surprising, as the largest matrix area fraction has the fewest inclusions, and so is closer to the dilute limit, where the D-EMT is virtually exact. However, even for the 0.3 matrix area fraction system, Fig. 5, the agreement is still very good. Tables 4 and 5 show the actual numbers in the graphs, for closer comparison and future reference. Note that as the matrix area fraction decreases, the moduli curves become steeper. This is because the shell area fraction (c_2) is becoming larger, and so changing its moduli has a greater effect on the overall moduli.

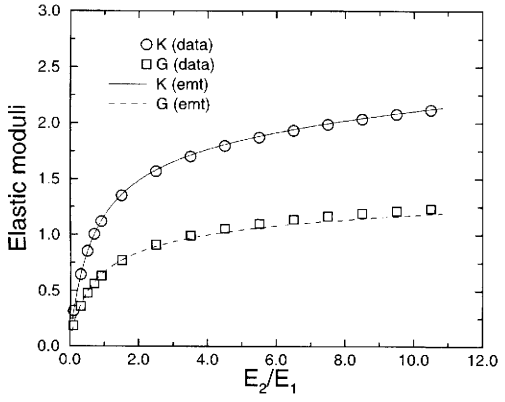

Fig. 5. Showing the D-EMT results for K and G compared to the numerical results for the 2D 0.3 matrix area fraction model.

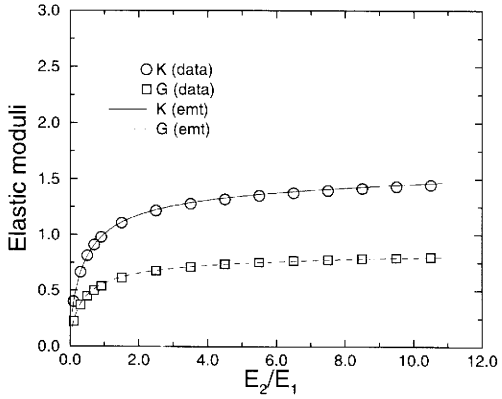

Fig. 6. Showing the D-EMT results for K and G compared to the numerical results for the 2D 0.5 matrix area fraction model.

Fig. 7 shows the comparision between D-EMT and finite element results for the 3D system with one size of inclusions. The agreement is excellent, as can also be seen in Table 6. Fig. 8 shows the same kind of comparison but for the two-size sphere 3D system. The agreement in this case between D-EMT and finite element data is almost as good as in Fig. 7. The data for this case are in

Table 4
A list of numerical data and D-EMT results for the 2D, 0.3 matrix area fraction system

E_2/E_1	K (data)	K (D-EMT)	G (data)	G (D-EMT)
0.1	0.320	0.319	0.186	0.187
0.3	0.645	0.643	0.364	0.378
0.5	0.855	0.854	0.479	0.495
0.7	1.005	1.006	0.564	0.580
0.9	1.120	1.123	0.631	0.644
1.5	1.351	1.360	0.772	0.775
2.5	1.568	1.580	0.910	0.897
3.5	1.702	1.714	0.995	0.971
4.5	1.797	1.809	1.055	1.023
5.5	1.872	1.883	1.101	1.063
6.5	1.935	1.944	1.138	1.096
7.5	1.988	1.997	1.168	1.123
8.5	2.036	2.044	1.194	1.147
9.5	2.079	2.086	1.216	1.168
10.5	2.119	2.125	1.236	1.186

Table 5
A list of numerical data and D-EMT results for the 2D, 0.5 matrix area fraction system

E_2/E_1	K (data)	K (D-EMT)	G (data)	G (D-EMT)
0.1	0.401	0.397	0.226	0.227
0.3	0.665	0.663	0.370	0.378
0.5	0.812	0.811	0.449	0.460
0.7	0.910	0.910	0.502	0.513
0.9	0.979	0.981	0.540	0.551
1.5	1.109	1.114	0.614	0.621
2.5	1.218	1.226	0.677	0.680
3.5	1.280	1.289	0.713	0.713
4.5	1.321	1.332	0.737	0.735
5.5	1.353	1.365	0.755	0.752
6.5	1.378	1.391	0.768	0.765
7.5	1.399	1.413	0.778	0.776
8.5	1.418	1.432	0.787	0.785
9.5	1.434	1.449	0.795	0.793
10.5	1.449	1.464	0.801	0.800

Table 6
A list of numerical data and D-EMT results for the 3D, 0.668 matrix volume fraction, one-sphere system (Fig. 7)

E_2/E_1	K (data)	K (D-EMT)	G (data)	G (D-EMT)
0.1	0.455	0.436	0.233	0.238
0.3	0.613	0.602	0.300	0.311
0.5	0.720	0.713	0.346	0.357
0.7	0.799	0.795	0.381	0.392
0.9	0.861	0.858	0.410	0.420
1.0	0.887	0.886	0.422	0.432
2.0	1.058	1.063	0.510	0.517
3.0	1.157	1.160	0.565	0.569
4.0	1.214	1.224	0.603	0.606
5.0	1.260	1.271	0.633	0.635
6.0	1.296	1.307	0.657	0.657
7.0	1.326	1.336	0.678	0.676
8.0	1.350	1.360	0.695	0.692
9.0	1.371	1.381	0.710	0.706
10.0	1.390	1.399	0.723	0.718

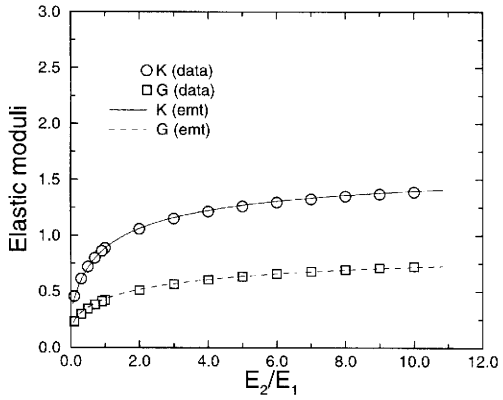

Fig. 7. Showing the D-EMT results for K and G compared to the numerical results for the monosize sphere 3D model. The matrix volume fraction is 0.668.

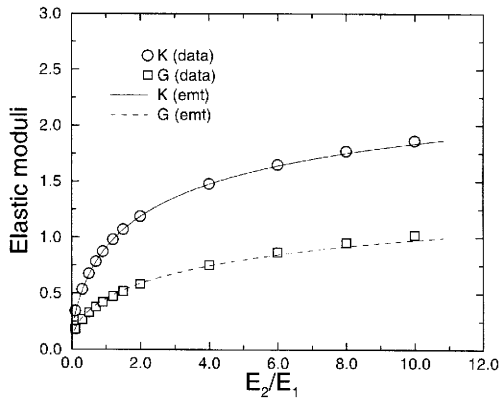

Fig. 8. Showing the D-EMT results for K and G compared to the numerical results for the two-size sphere 3D model. The matrix volume fraction is 0.517.

Table 7. It should be recalled here that the finite element results for the two-size sphere 3D system were not checked as thoroughly as were the other systems, so there could be a larger degree of error in these results. It was found in the one-size sphere 3D system that increasing the system size for the larger values of E_2 tended to decrease the overall moduli. If the numerical results in Fig. 8 were to drop by only a few percent, the already good agreement with the D-EMT results would be substantially improved.

5. Discussion and summary

One limitation of the D-EMT equations is our ability (or inability) to match the microstructure of composites (Torquato, 2001). In concrete, for example, several modeling and experimental studies have shown that in a typical concrete, the shell regions are themselves overlapping and percolating (Winslow et al., 1994; Bentz et al., 1999; Scrivener and Nemati, 1996). The form of D-EMT considered in this paper does not reflect this fact.

Table 7
A list of numerical data and D-EMT results for the 3D, 0.517 matrix volume fraction, two-sphere system (Fig. 8)

E_2/E_1	K (data)	K (D-EMT)	G (data)	G (D-EMT)
0.1	0.346	0.327	0.183	0.189
0.3	0.537	0.526	0.269	0.283
0.5	0.676	0.668	0.331	0.346
0.7	0.785	0.779	0.381	0.396
0.9	0.874	0.869	0.423	0.437
1.2	0.983	0.980	0.476	0.487
1.5	1.071	1.075	0.521	0.533
2.0	1.189	1.187	0.584	0.589
4.0	1.479	1.475	0.755	0.746
6.0	1.650	1.639	0.868	0.846
8.0	1.772	1.753	0.953	0.919
10.0	1.866	1.837	1.022	0.975

The model microstructures used to test the D-EMT, therefore, were carefully constructed to have non-overlapping and therefore non-percolating shell regions. However, whether or not percolation of a phase significantly affects the overall properties depends on the contrast of its properties with those of the surrounding phases (Shane et al., 2000; Garboczi et al., 1995). In concrete, the shell moduli are less than the matrix moduli by a factor of at most 2–3, which is not enough contrast for percolation to be important (Shane et al., 2000). So this deficiency in D-EMT should not significantly affect the accuracy of D-EMT for the concrete problem (Garboczi and Berryman, 2000).

The exact effect of this aspect of the D-EMT was explored by creating a microstructure like that shown in the lefthand side of Fig. 2. The same number and type of inclusions were used, but now the shells were allowed to be overlapping, although phase 3, the inclusions, were still not allowed to overlap. There was therefore the same area fraction for phase 3, but the matrix area fraction was 0.340, instead of 0.303, and the shell area fraction became 0.238, instead of 0.275. The shell overlaps caused a somewhat smaller shell area fraction, and thus a larger matrix area fraction.

Fig. 9 shows the numerical results, along with two sets of D-EMT results. The first, the dashed lines, are just the D-EMT results shown in Fig. 5. These actually work quite well, with a maximum

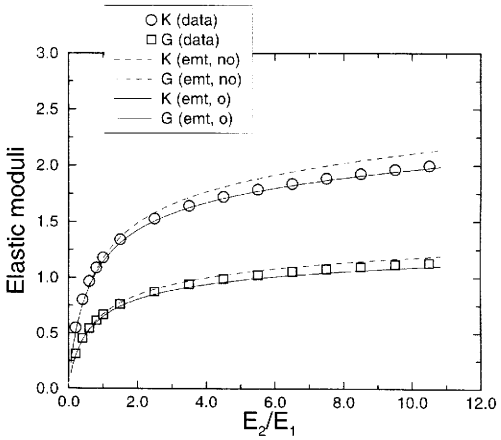

Fig. 9. Showing the D-EMT and numerical results for K and G for the system when the shells were allowed to overlap. The matrix area fraction is 0.340. The dashed lines are the D-EMT results from the non-overlapping (no) shell case. The solid lines are the D-EMT results for the overlapping (o) case, where the true matrix area fraction was used (0.340 instead of 0.303).

error of less than 10% at the highest values of E_2/E_1. Most real concrete materials have $0.1 < E_2/E_1 < 2.0$, and in this region the D-EMT compares well with the numerical results. The second set of D-EMT results is for the case of a matrix area fraction of 0.340, which matches the real microstructure. In the numerical solution of the D-EMT equations, the variable is the matrix area fraction, so it makes sense to use the actual known value for the overlapping shell microstructure. In this case, there is significantly better agreement with the numerical results, as good as that seen in Fig. 5.

In the 2D models, the shell thickness was such that the shell area fraction was comparable to the matrix area fraction. This is why there was a significant difference in area fractions between the non-overlapping and overlapping shell microstructures. This would be the case also in the 3D models considered as well. However, in most concrete materials, the shell is very thin compared to the inclusion diameters. The difference between non-overlapping and overlapping shell volume fractions would be quite small. Fig. 10 shows, for a typical concrete aggregate (inclusion) particle size distribution, the shell volume fraction if the shells are considered to be non-overlapping, and the

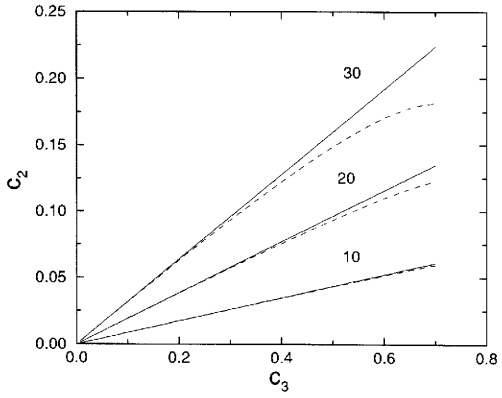

Fig. 10. Showing the shell volume fraction, c_2, vs. the inclusion volume fraction, c_3, for a 3D case where the size distribution of the particles was that of the aggregates in a typical concrete mixture. The three sets of curves are labeled with the thickness of the shell phase in micrometers. The solid curves are the shell volume fractions assuming no overlaps, while the dashed curves are the Lu-Torquato estimate, which has been shown to be very accurate for overlapping shells.

overlapping shell volume fraction as given by the Lu–Torquato formulae (Lu and Torquato, 1992), plotted vs. the volume fraction of the aggregate, which is the only phase volume fraction that is precisely known in concrete. The Lu–Torquato formulae have been shown to be very accurate for concrete problems (Garboczi and Bentz, 1997; Garboczi and Bentz, 1998). The aggregate volume fraction in concrete is typically from 60% to 70%. Since the three-phase model thickness of the ITZ in most concrete materials is 20 μm or less, it is seen that there is little difference between the shell volume fraction for the two cases, which implies that the fact of shell overlap in real concrete will not make much difference to the utility of the D-EMT equations in the elastic case.

Since EMT is an uncertain approximation (having relatively crude control of the underlying microstructure), the results of this paper are especially important in carefully showing the expected accuracy of the D-EMT equations. We have shown that the new form of D-EMT worked very well for the class of problems considered. Checking the D-EMT against models for a material like concrete, where the particle size distribution of the inclusions is quite a bit larger (about two orders of magnitude) than that studied here, has not been done. The main difficulty comes in finding a numerical representation of the inclusion structure using a digital image. The pixel width must be at most 5 μm, in order to barely resolve the 20 μm ITZ regions. To look at even a 1000 mm^3 cubic sample, which is small for concrete, a 2000^3 model must be considered, which would require 1600 GB of memory, and require weeks or months of CPU time to run (Garboczi, 1998). This run time would of course be diminished by using massively parallel computers, and the memory required could be reduced by using an adaptive meshing scheme, to optimize the finite element mesh and so use fewer elements. The errors incurred using the D-EMT for a material like concrete could be significantly larger. But the excellent agreement with the numerical data found here strongly suggests that successful extensions to concrete are possible.

Tables 4–7 in this paper should be useful for other researchers who wish to test various forms of EMT or other approximate formulas, by listing accurate data for the linear elastic properties of non-trivial random systems. Using the information contained in Tables 1–3, the microstructures can be recreated easily, in case new numerical methods need to be tested. Modern computers and computer methods can now be used for the quantitative testing of approximate micromechanics theories on non-trivial, non-analytic microstructures. This will allow a better sorting of various equations into areas of greatest usefulness, and should inspire the creation of better, more accurate choices among the various theories available now (Torquato, 2001) and possible in the future.

Acknowledgements

We thank the Partnership for High Performance Concrete Technology of the Building and Fire Research Laboratory for partial support of the work of EJG, and the National Science Foundation Science and Technology Center for Advanced Cement-Based Materials for supporting an Annual Computer Modeling Workshop (see http://ciks.cbt.nist.gov/monograph/) at which the

authors first began to formulate their new differential effective medium theory ideas. The work of JGB was performed under the auspices of the U.S. Department of Energy by the University of California Lawrence Livermore National Laboratory under contract No. W-7405-ENG-48 and supported specifically by the Geosciences Research Program of the DOE Office of Energy Research within the Office of Basic Energy Sciences, Division of Engineering and Geosciences.

References

Bentz, D.P., Stutzman, P.A., Garboczi, E.J., 1992. Experimental and simulation studies of the interfacial zone in concrete. Cem. Conc. Res. 22, 891–902.

Bentz, D.P., Garboczi, E.J., Stutzman, P.A., 1993. Computer modelling of the interfacial transition zone in concrete. In: Maso, J.C. (Ed.), Interfaces in Cementitious Composites. E. & F.N. Spon, London, 1993, pp. 259–268. Also found at http://ciks.cbt.nist.gov/monograph/, Part I, Chapter 6, Section 3.

Bentz, D.P., Garboczi, E.J., Lagergren, E.S., 1998. Multi-scale microstructural modelling of concrete diffusivity: identification of significant variables. Cem., Conc., Aggregates 20, 129–139.

Bentz, D.P., Garboczi, E.J., Snyder, K.A., 1999. A hard-core soft shell microstructural model for studying percolation and transport in three-dimensional composite media. NIST Internal Report 6265. Also available at http://ciks.cbt.nist.gov/monograph/, Part I, Chapter 6, Section 8.

Berge, P.A., Berryman, J.G., Bonner, B.P., 1993. Influence of microstructure on rock elastic properties. Geophys. Res. Lett. 20, 2619–2622.

Berryman, J.G., 1995. Mixture theories for rock properties. In: Ahrens, T.J. (Ed.), Rock Physics and Phase Relations – A Handbook of Physical Constants. American Geophysical Union, Washington, DC, pp. 205–228.

Christensen, R.M., 1979. Mechanics of Composite Materials. Wiley, New York, pp. 47–58.

Christensen, R.M., 1990. A critical evaluation for a class of micromechanics models. J. Mech. Phys. Solids 38, 379–404.

Christensen, R.M., Lo, K.H., 1979. Solutions for effective shear properties in three phase sphere and cylinder models. J. Mech. Phys. Solids 27, 315–330.

Cleary, M.P., Chen, I.W., Lee, S.M., 1980. Self-consistent techniques for heterogeneous media. J. Eng. Mech. Div. – ASCE 106, 861–887.

Cooper, D.W., 1988. Random-sequential-packing simulations in three dimensions for spheres. Phys. Rev. A 38, 522–524.

Douglas, J.F., Garboczi, E.J., 1995. Intrinsic viscosity and polarizability of particles having a wide range of shapes. Adv. Chem. Phys. 91, 85–153.

Dvorkin, J., Berryman, J., Nur, A., 1999. Elastic moduli of cemented sphere packs. Mech. Mater. 31, 461–469.

Garboczi, E.J., 1998. Finite element and finite difference programs for computing the linear electric and elastic properties of digital images of random materials. NIST Internal Report 6269. Also available at http://ciks.cbt.nist.gov/monograph/, Part II, Chapter 2.

Garboczi, E.J., Bentz, D.P., 1991. Digital simulation of the aggregate-cement paste interfacial zone in concrete. J. Mater. Res. 6, 196–201.

Garboczi, E.J., Bentz, D.P., 1997. Analytical formulas for interfacial transition zone properties. Adv. Cem.-Based Mater. 6, 99–108.

Garboczi, E.J., Bentz, D.P., 1998. Multi-scale analytical/numerical theory of the diffusivity of concrete. Adv. Cem.-Based Mater. 8, 77–88.

Garboczi, E.J., Berryman, J.G., 2000. New effective medium theory for the diffusivity or conductivity of a multi-scale concrete microstructure model. Conc. Sci. Eng. 2, 88–96.

Garboczi, E.J., Day, A.R., 1995. An algorithm for computing the effective linear elastic properties of heterogeneous materials: 3-D results for composites with equal phase Poisson ratios. J. Mech. Phys. Solids 43, 1349–1362.

Garboczi, E.J., Snyder, K.A., Douglas, J.F., Thorpe, M.F., 1995. Geometrical percolation threshold of overlapping ellipsoids. Phys. Rev. E 52, 819–828.

Garboczi, E.J., 2001. http://ciks.cbt.nist.gov/monograph, Part II, Chapter 7, Section 7.

Hashin, Z., 1962. The elastic moduli of heterogeneous materials. J. Appl. Mech. 29, 143–150.

Herve, E., Zaoui, A., 1993. *n*-Layered inclusion-based micromechanical modelling. Int. J. Eng. Sci. 31, 1–10.

Hildebrand, F.B., 1956. Introduction to Numerical Analysis. Dover, New York, pp. 285–292.

Hill, R., 1963. Elastic properties of reinforced solids: Some theoretical principles. J. Mech. Phys. Solids 11, 357–372.

Iske, P.L., Sterk, N.K.J., Oortwijn, J., 1994. Effective elastic properties of suspensions of radially symmetric particles. Physica A 209, 96–128.

Lu, B., Torquato, S., 1992. Nearest-surface distribution functions for polydispersed particle systems. Phys. Rev. A 45, 5530–5544.

Lutz, M.P., Monteiro, P.J.M., 1995. Effect of the transition zone on the bulk modulus of concrete. In: Diamond, S., Mindess, S., Glasser, F.P., Roberts, L.W., Skalny, J.P., Wakeley, L.D. (Eds.), Microstructure of Cement-Based Systems/Bonding and Interfaces in Cementitious Materials, vol. 370. Materials Research Society, Pittsburgh, pp. 413–418.

McLaughlin, R., 1977. A study of the differential scheme for composite materials. Int. J. Eng. Sci. 15, 237–244.

Milton, G.W., 1985. The coherent potential approximation is a realizable effective medium scheme. Commun. Math. Phys. 99, 463–500.

Norris, A.N., 1985. A differential scheme for the effective moduli of composites. Mech. Mater. 4, 1–16.

Ostoja-Starzewski, M., Jasiuk, I., Wang, W., Alzebdeh, K., 1996. Composites with functionally graded interphases:

mesocontinuum concept and effective transverse conductivity. Acta Mater. 44, 2057–2066.

Ostoja-Starzewski, M., Schulte, J., 1996. Bounding of effective thermal conductivities of multiscale materials by essential and natural boundary conditions. Phys. Rev. B 54, 278–285.

Press, W.H., Flannery, B.P., Teukolsky, S.A., Vetterling, W.T., 1988. Numerical Recipes in C. Cambridge University Press, Cambridge, pp. 566–573.

Roberts, A.P., Garboczi, E.J., 2000. Elastic properties of model porous ceramics. J. Amer. Ceram. Soc. 83, 3041 3048.

Schwartz, L.M., Garboczi, E.J., Bentz, D.P., 1995. Interfacial transport in porous media: application to D.C. electrical conductivity of mortars. J. Appl. Phys. 78, 5898–5908.

Scrivener, K.L., 1989. The microstructure of concrete. In: Skalny, J. (Ed.), Materials Science of Concrete, vol. I. American Ceramic Society, Westerville, OH, pp. 127 162.

Scrivener, K.L., Nemati, K.M., 1996. The percolation of pore space in the cement paste/aggregate interfacial zone of concrete. Cem. Conc. Res. 26, 35–40.

Shane, J.D., Mason, T.O., Jennings, H.M., Garboczi, E.J., Bentz, D.P., 2000. Effect of the interfacial transition zone on the conductivity of portland cement mortars. J. Amer. Ceram. Soc. 83, 1137–1144.

Sheng, P., 1990. Effective medium theory of sedimentary rocks. Phys. Rev. B 41, 4507–4512.

Sheng, P., 1991. Consistent modeling of the electrical and elastic properties of sedimentary rocks. Geophysics 56, 1236–1243.

Sheng, P., Callegari, A.J., 1984. Differential effective medium theory of sedimentary rocks. Appl. Phys. Lett. 44, 738–740.

Torquato, S., 1991. Random heterogeneous media: microstructure and improved bounds on effective properties. Appl. Mech. Rev. 44, 37–76.

Torquato, S., 2001. Theory of Composite Materials. Oxford University Press, London.

Winslow, D.N., Cohen, M.D., Bentz, D.P., Snyder, K.A., Garboczi, E.J., 1994. Percolation and porosity in mortars and concretes. Cem. Conc. Res. 24, 25–37.

Xia, W., Thorpe, M.F., 1988. Percolation properties of random ellipses. Phys. Rev. A 38, 2650.